

THE COMPOSITION OF CHRYSOTILE AND ITS RELATIONSHIP WITH LIZARDITE

DAVID S. O'HANLEY¹

Trinity School at River Ridge, 2300 E. 88th Street, Bloomington, Minnesota 55425, U.S.A.

M. DARBY DYAR*

Department of Geology and Astronomy, West Chester University, West Chester, Pennsylvania 19383, U.S.A.

ABSTRACT

Mössbauer data were obtained from 14 specimens of chrysotile taken from three geologically well-characterized serpentinites. These data were used in conjunction with results of electron-microprobe (major elements) and uranium-extraction analyses (H_2O) to generate a comprehensive set of compositions for chrysotile. Chrysotile contains both Al and Fe^{3+} as secondary tetrahedrally coordinated cations, with Al dominating over Fe^{3+} . The proportion of $^{54}Fe^{3+}$ and $^{56}Fe^{3+}$ shows an inverse correlation that preserves a relatively constant total Fe^{3+} content. Most specimens have low Fe^{3+}/Fe^{2+} . The incorporation of trivalent cations is greater in the sheet of octahedra than in the sheet of tetrahedra, suggesting the presence of H^+ vacancies; this result is consistent with measured H_2O contents. The Mössbauer parameters for chrysotile are similar but more scattered than those for lizardite, suggesting minimal differences in coordination polyhedra between the two minerals. However, chrysotile and lizardite are not polymorphs in natural systems. Compared to the associated lizardite, chrysotile contains more Fe^{2+} and ^{54}Al and fewer $^{54}Fe^{3+}$ ions and H^+ vacancies. These data support the hypothesis that high Fe^{2+} content and H^+ vacancies contribute to the replacement of lizardite by chrysotile, and *vice versa*, during serpentine replacement.

Keywords: chrysotile, Mössbauer spectroscopy, electron-microprobe data, uranium-extraction analysis, lizardite, phase relations, serpentine replacement, serpentinization.

SOMMAIRE

Nous avons caractérisé par spectroscopie de Mössbauer quatorze échantillons de chrysotile prélevés de trois exemples de serpentinite dont le contexte géologique est bien établi. Ces données ont servi, avec les résultats d'analyses à la microsonde (éléments majeurs) et par extraction à l'uranium (H_2O), à établir une collection de compositions complètes pour le chrysotile. Cette espèce contient à la fois Al et Fe^{3+} comme ions secondaires dans le site à coordination tétraédrique, avec Al en prédominance. Les proportions de $^{54}Fe^{3+}$ et de $^{56}Fe^{3+}$ montrent une corrélation inverse qui mène à une teneur relativement constante de la teneur globale en Fe^{3+} . La plupart des échantillons ont un faible rapport Fe^{3+}/Fe^{2+} . L'incorporation des ions trivalents est plus importante dans le feuillet d'octaèdres que dans le feuillet de tétraèdres, ce qui indiquerait la présence de lacunes dans le site H^+ ; ce phénomène expliquerait bien les teneurs en H_2O mesurées. Les spectres de Mössbauer du chrysotile ressemblent à ceux de la lizardite, mais ils sont plus irréguliers, ce qui fait penser que les différences impliquant les polyèdres de coordination entre ces deux minéraux sont assez subtiles. Il est toutefois évident que chrysotile et lizardite ne sont pas des polymorphes dans les systèmes naturels. Par rapport à la lizardite coexistante, le chrysotile contient davantage de Fe^{2+} et de ^{54}Al , et moins de $^{54}Fe^{3+}$ et de lacunes dans les sites H^+ . Ces données étayent l'hypothèse d'un remplacement de la lizardite par le chrysotile là où la teneur en Fe^{2+} et le taux de lacunes dans la position H^+ sont favorisés, et *vice versa*, dans les cas de remplacement de serpentines.

(Traduit par la Rédaction)

Mot-clés: chrysotile, spectroscopie de Mössbauer, données de microsonde électronique, analyses par extraction à l'uranium, lizardite, relations de phase, remplacement de serpentines, serpentinisation.

¹ E-mail address: ohanleys@aol.com

* Now at the Department of Geography and Geology, Mount Holyoke College, South Hadley, Massachusetts 01075, U.S.A.
E-mail address: mddyar@amherst.edu

INTRODUCTION

Historically, the central problem in studies of serpentine-group minerals deals with the compositional relationship among lizardite, chrysotile, and antigorite: why do three distinct structural arrangements exist for similar compositions (Whittaker & Zussman 1956)? The studies of Whittaker & Wicks (1970), Evans *et al.* (1976), and Mellini *et al.* (1987) show that the modulated structure of antigorite imparts a distinct composition to it (less MgO and H₂O, because of absences of Mg octahedra) compared to lizardite and chrysotile, such that antigorite is not truly a polymorph of the other two. Typically, this compositional difference is not discernible in electron-microprobe data (Wicks & Plant 1979, Mellini *et al.* 1987, O'Hanley & Wicks 1995). The compositional relationship between lizardite and chrysotile is uncertain.

O'Hanley (1991) and O'Hanley & Wicks (1995) demonstrated that the parageneses of lizardite and chrysotile in serpentinites are consistently distinct, but they could not present an unequivocal explanation of the compositional differences between lizardite and chrysotile. Our study of lizardite 1T (O'Hanley & Dyar 1993), based on a synthesis of electron-microprobe data and Mössbauer spectroscopic analyses, demonstrated the role of Fe³⁺ in the petrogenesis of lizardite, and provided an explanation of some of the petrographic observations concerning lizardite reported by Cogulu & Laurent (1984) and O'Hanley & Wicks (1995). The compositional data for chrysotile was limited to a few specimens only, which precluded any conclusions concerning its behavior during serpentinization.

Included in this paper are better-documented mineral compositions of chrysotile. This dataset, which couples results of electron-microprobe and Mössbauer spectroscopic analyses, shows that the different parageneses of lizardite and chrysotile result from differential partitioning of Fe³⁺ and Fe²⁺ between different sites in the two minerals. It is our goal in this paper to demonstrate these differences, and to propose an explanation for the complex parageneses of lizardite and chrysotile.

GEOLOGICAL SETTING OF THE SAMPLES SELECTED

The specimens of chrysotile chosen for this study were taken from the same serpentinites used as sources of lizardite by O'Hanley & Dyar (1993) because: 1) these serpentinites are well characterized, and 2) such a choice facilitates comparison of chrysotile with lizardite within the same serpentinite. The characteristics of these serpentinites are summarized by O'Hanley & Dyar (1993), and are described in the following papers: the Woodsreef serpentinite by Glen & Butt (1981) and O'Hanley & Offler (1992), the Jeffrey serpentinite by O'Hanley & Wicks (1990), and the Cassiar serpentinite by O'Hanley *et al.* (1992) and O'Hanley & Wicks

(1995). Each of these serpentinites has features that are significant for this study: 1) formation temperatures at or below 300°C, with formation at constant (Cassiar) or decreasing (Woodsreef) temperature, 2) slight differences in bulk-rock compositions, with Jeffrey serpentinites possessing lower SiO₂ contents than those at Cassiar, which are lower than those at Woodsreef, and 3) complex paragenetic relations between lizardite and chrysotile.

As a group, the specimens represent three distinct occurrences of chrysotile. The most familiar of these is veins of chrysotile asbestos (labeled asbestos in Table 1), in which chrysotile fills fractures that are continuous on the scale of at least several grains of olivine (Fig. 1A). The second occurrence is veins of "picrolite" (Fig. 1B), a field term that describes any vein of serpentine that is typically apple green in color and either massive or pseudofibrous in appearance. Although "picrolite" can consist of any one of the serpentine minerals (*e.g.*, Wicks 1979, Mellini & Zussman 1986), the specimens used here have been identified as consisting of chrysotile on the basis of X-ray-diffraction experiments. The third occurrence has been termed "bastite fiber" (Glen & Butt 1981), an occurrence characterized by discrete lenses of chrysotile asbestos within individual grains of serpentinized pyroxene (Fig. 1C).

EXPERIMENTAL METHODS

Mineral assemblages were identified optically on the basis of results of Wicks & Plant (1979) and by microbeam X-ray diffraction using the methodology of Wicks & Zussman (1975). Samples of chrysotile are easy to obtain from asbestos veins. For other specimens, mineral separates were removed from thin sections with a drill. Fourteen specimens of chrysotile were chosen from the three occurrences of serpentinite mentioned. Data for two specimens of chrysotile from Cassiar (C167 and C200), reported by O'Hanley & Dyar (1993), also are included. Several samples (all from the Jeffrey serpentinite) containing significant amounts of brucite, identified by petrographic observation, microbeam X-ray diffraction, or analyses of structural H₂O between 16 and 20% H₂O, were rejected. Purity of samples is estimated to be close to 100% chrysotile with or without magnetite.

Electron-microprobe data (Table 1) for the serpentine minerals were obtained using a JEOL 8600 Superprobe housed at the University of Saskatchewan; natural mineral standards, including a serpentine for Mg and Si, were used under operating conditions of 15 kV and 10 nA. Collection times varied from 20 to 60 s per element. Longer collecting times did not improve significantly either oxide totals or cation ratios. Analyses of chrysotile are difficult for two reasons (Wicks & Plant 1979). Firstly, chrysotile asbestos may either compress or shed fibers as the section is polished,

TABLE 1. SAMPLE DESCRIPTIONS AND RESULTS OF ELECTRON-MICROPROBE AND URANIUM-EXTRACTION ANALYSES (wt%) OF CHRYSOTILE SPECIMENS

Sample	Description*	SiO ₂	Al ₂ O ₃	Cr ₂ O ₃	FeO	MgO	MnO	NiO	H ₂ O	Total†
Cassiar Serpentinite										
C54	asb vein, cuts lz hrgls	40.11	3.44	0.03	2.55	39.76	0.06	0.00	11.83	98.17
Woodsreef Serpentinite										
W6	asb vein, silky, cuts hrgls	39.29	3.34	0.66	2.78	38.34	0.09	0.04	12.43	97.11
W8	asb vein, silky, cuts hrgls	35.68	1.66	0.00	2.21	34.95	0.00	0.00	12.06	86.67
W10	asb vein, silky, cuts hrgls	42.17	2.90	0.05	3.73	40.44	0.09	0.05	12.02	101.58
W10	bastite fiber, ntck	41.20	1.30	0.00	3.61	38.94	0.09	0.01	12.65	97.95
W11	asb vein, silky, cuts hrgls	40.05	2.07	0.14	3.33	38.42	0.09	0.08	11.79	96.15
W15	picrolite vein	39.97	2.74	0.13	2.97	37.95	0.06	0.02	11.76	95.72
W15	asb vein, silky, cuts hrgls	41.69	3.19	0.01	3.70	39.61	0.08	0.02	12.24	100.67
W54	asb vein, semi-harsh fiber	40.39	3.68	0.00	3.08	39.91	0.05	0.00	11.99	99.25
W54	pic vein, cuts lz hrgls	40.69	3.38	0.00	3.47	39.63	0.06	0.02	12.31	100.20
W70	pic vein, cuts lz hrgls	40.12	2.94	0.01	3.42	40.46	0.08	0.04	12.61	99.82
W96	pic vein, cuts lz hrgls	41.97	2.27	0.00	2.83	40.20	0.05	0.10	12.30	99.85
Jeffrey Serpentinite										
J60-2	asb, mass fiber	41.67	3.36	0.00	1.69	40.97	0.04	0.20	12.21	100.24
J68	asb vein, cuts atg-lz-ctl ntck	40.37	1.50	0.01	1.54	41.08	0.12	0.04	12.12	96.92

*abbreviations under description are: asb = asbestos; lz = lizardite; hrgls = hourglass; ntck = interlocking textures; pic = picrolite; atg = antigorite; ctl = chrysotile.

†TiO₂, CaO, Na₂O, and K₂O less than 0.05 wt% each, but total includes them.

resulting in both cases in irregular surfaces polished to varying degrees. Secondly, chrysotile does not polish well even where it is not fibrous.

Chrysotile mineral formulas were calculated on the basis of 14 atoms of oxygen (Table 2). Based on the Mössbauer data, the FeO values were recast as either Fe²⁺ or Fe³⁺ and assigned to sites. Al was used to fill tetrahedral sites, and the remaining Al was assigned to octahedra. If the total of the octahedrally coordinated cations deviated from 6.000 by less than 1% (between 5.95 and 6.05), the analysis was accepted. In most cases, results of analyses (Table 1) represent averages.

Samples were analyzed for H₂O contents in the Stable Isotope Laboratory at Southern Methodist University using the uranium-extraction method of Bigeleisen *et al.* (1952) and Holdaway *et al.* (1986). The values vary between 11.8 and 12.9% H₂O, with one value at 13.4 wt% H₂O (Table 1). These data were combined with the electron-microprobe results to calculate mineral formulas based on 18 atoms of oxygen. Only the H⁺ contents and the excess charges are shown in Table 2.

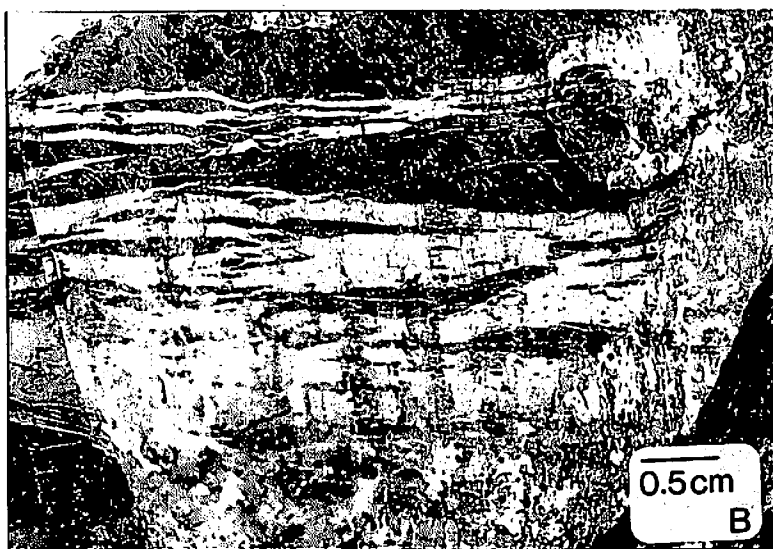
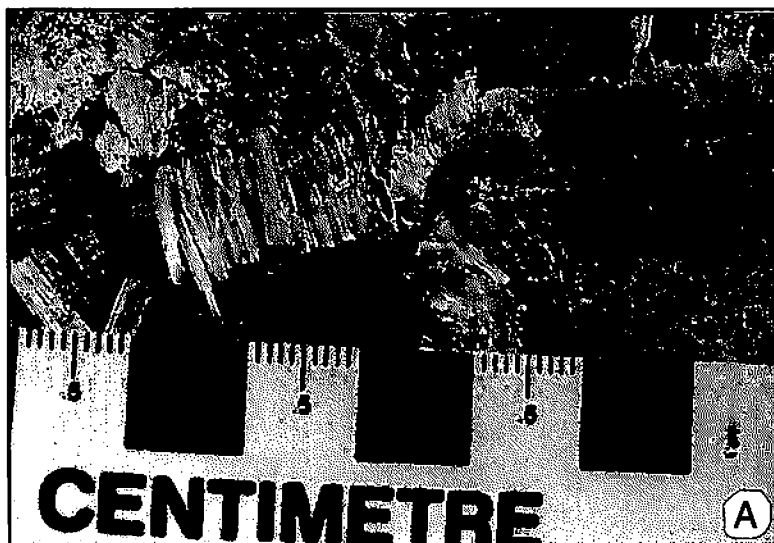
Room-temperature Mössbauer studies to determine Fe²⁺ and Fe³⁺ content were done in the Mineral Spectroscopy Laboratory at West Chester University, with some of the earlier analyses done at the University of Oregon. Sample thicknesses ranged from 1–2 mg

Fe/cm² calculated using the method of Long *et al.* (1984) (see complete discussion in Grant 1995). There was insufficient sample available to evaluate a possible thickness (saturation) correction; however, experience with amphibole (Skogby *et al.* 1992, Grant 1995) suggests that its magnitude could be approximately 1% of the total spectral area for each doublet fit. Fitting procedures in general followed those described in O'Hanley & Dyar (1993).

RESULTS

All but one of the chrysotile samples (specimen J68 chrysotile, Table 3) analyzed during this study contain ¹⁴Fe³⁺, on the basis of the high-energy peak of the ¹⁴Fe³⁺ doublet that is visible in the spectra near 0.35 mm/s (Fig. 2). In the spectrum for sample C54 (Fig. 2A), the peaks for both ¹⁴Fe³⁺ and ¹⁶Fe³⁺ are clearly visible; in the spectrum for chrysotile W10 (Fig. 2B), the peaks for ¹⁴Fe³⁺ and ¹⁶Fe³⁺ are smaller relative to Fe²⁺ peaks, but are still discernible in view of the asymmetry of the Fe²⁺ peak shape in the spectrum.

The values for isomer shift (δ) and quadrupole splitting (Δ) measured for chrysotile in this study (Table 3) are more variable than, but overlap with, those of lizardite (O'Hanley & Dyar 1993; see bottom lines of Table 3), suggesting minimal differences in the geometry of coordination polyhedra between chrysotile and lizardite.



In the tetrahedrally coordinated site, ^{14}Al predominates over $^{14}\text{Fe}^{3+}$ (Fig. 3A). The proportion of Cr is low (Fig. 3B), and $^{16}\text{Fe}^{3+}$ and ^{16}Al are not correlated (Fig. 3B). There is an inverse correlation between $^{14}\text{Fe}^{3+}$ and $^{16}\text{Fe}^{3+}$ (Fig. 3C), and the total Fe^{3+} content is approximately constant in these specimens. The proportions of Fe^{2+} and $^{16}\text{Fe}^{3+}$ show a slight inverse correlation (Fig. 3D), whereas the amount of Fe^{2+} shows a strong inverse correlation with that of Mg (Fig. 3E). $^{16}\text{Fe}^{3+}$ is not correlated with Mg (Fig. 3E).

Two differences in composition are apparent among chrysotile samples from the three bodies of serpentinite. Firstly, the chrysotile samples from Woodsreef contain between 0.20 and 0.29 atoms of Fe per 14 atoms of oxygen, whereas those from Jeffrey contain 0.12 and 0.13 atoms of Fe (Table 2). The chrysotile samples from Cassiar contain intermediate amounts of Fe. Secondly, the Woodsreef specimens contain the lowest amounts of Mg. On the basis of 14 atoms of oxygen, all but two have excess charge that is

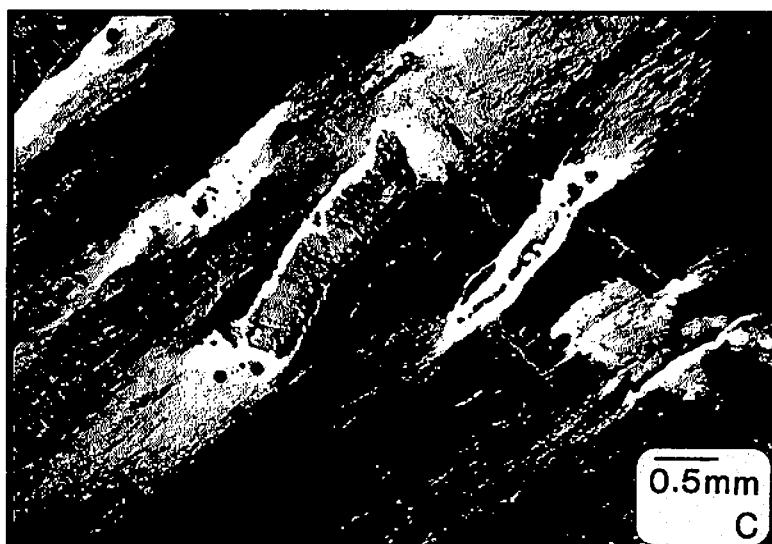


FIG. 1. Examples of chrysotile specimens used in this study. A. Vein of chrysotile asbestos (British Canadian mine). B. Veins of picrolite (Woodsreef serpentinite). C. Photomicrograph of bastite fiber (Woodsreef serpentinite).

TABLE 2. COMPOSITIONS (apfu) FOR CHRYSOTILE SPECIMENS

	Si	¹⁴ Fe ³⁺	¹⁴ Al	¹⁸ Fe ³⁺	¹⁸ Al	14 O Basis* Cr	¹⁸ Fe ²⁺	Mg	Mn	Ni	Excess Charge†	18 O Basis* H	Excess Charge†
Cassiar Serpentine													
C54	3.79	0.042	0.162	0.092	0.221	0.002	0.088	5.606	0.005	0.013	0.109	7.551	0.191
C167‡	3.97	0.040	n.a.	0.050	0.050	0.000	0.040	5.780	n.a.	n.a.	0.060	n.a.	n.a.
C200‡	3.95	0.030	0.020	0.050	0.030	0.000	0.030	5.820	n.a.	n.a.	0.030	n.a.	n.a.
Woodsreef Serpentine													
W6	3.80	0.043	0.159	0.031	0.220	0.050	0.150	5.521	0.007	0.003	0.186	7.991	0.078
W8	3.89	0.028	0.078	0.026	0.135	0.000	0.148	5.685	0.000	0.000	0.055	8.579	-0.127
W10asb	3.85	0.034	0.109	0.046	0.203	0.004	0.205	5.512	0.007	0.000	0.118	7.454	0.244
W10	3.95	0.046	n.a.	0.046	0.147	0.000	0.197	5.570	0.007	0.001	0.137	8.055	0.104
W11	3.89	0.038	0.072	0.043	0.164	0.011	0.169	5.560	0.007	0.007	0.109	7.694	0.176
W15	3.88	0.020	0.096	0.050	0.165	0.010	0.170	5.500	0.005	0.002	0.160	7.687	0.231
W15asb	3.86	0.060	0.081	0.000	0.266	0.001	0.220	5.462	0.007	0.002	0.126	7.635	0.212
W54asb	3.78	0.080	0.136	0.000	0.269	0.000	0.170	5.572	0.004	0.000	0.054	7.582	0.149
W54	3.79	0.030	0.175	0.080	0.145	0.000	0.160	5.503	0.005	0.001	0.120	7.701	0.168
W70	3.78	0.067	0.156	0.027	0.169	0.001	0.175	5.676	0.006	0.003	-0.027	7.914	-0.030
W96	3.91	0.018	0.075	0.059	0.174	0.000	0.143	5.577	0.004	0.007	0.140	7.698	0.205
Jeffrey Serpentine													
J60-2	3.84	0.030	0.131	0.020	0.233	0.000	0.081	5.625	0.002	0.015	0.093	7.595	0.193
J68	3.87	0.000	0.130	0.080	0.039	0.000	0.040	5.867	0.010	0.003	-0.011	7.783	0.027

*Mineral compositions calculated two ways: (1) 14 oxygens, without H₂O; (2) 18 oxygens, including H₂O.

†Excess charge is the sum of octahedrally coordinated trivalent cations minus the total of tetrahedrally coordinated trivalent cations.

‡Compositions from O'Hanley & Dyar (1993).

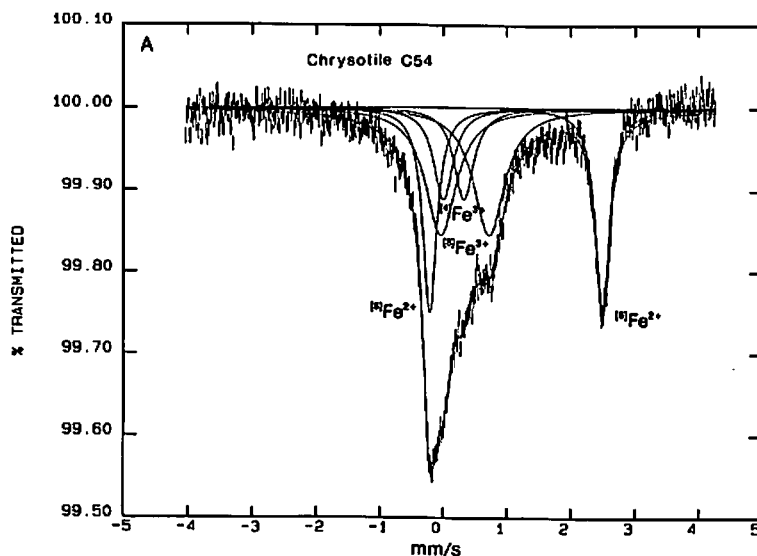
N.a. = not analyzed.

TABLE 3. MÖSSBAUER PARAMETERS (mm/s) FOR CHRYSOTILE SPECIMENS

Sample	$^{56}\text{Fe}^{2+}$				$^{56}\text{Fe}^{3+}$				$^{57}\text{Fe}^{3+}$				Statistics*		Percent of total Fe		
	δ_1	Δ_1	Γ_1	A_1	δ_2	Δ_2	Γ_2	A_2	δ_3	Δ_3	Γ_3	A_3	%Mis	%Uncrt	$^{56}\text{Fe}^{2+}$	$^{56}\text{Fe}^{3+}$	$^{57}\text{Fe}^{3+}$
C54	1.14	2.71	0.26	33	0.34	0.76	0.59	46	0.16	0.32	0.37	21	0.31	0.03	33	46	21
W6	1.14	2.71	0.26	67	0.35	0.99	0.79	14	0.10	0.34	0.54	19	0.41	0.05	67	14	19
W8	1.13	2.73	0.26	68	0.32	0.99	0.46	12	0.18	0.30	0.46	13	1.46	0.07	73	13	14
W10asb	1.13	2.71	0.26	72	0.35	0.89	0.66	16	0.18	0.25	0.50	12	0.27	0.02	72	16	12
W10bas	1.14	2.71	0.25	68	0.35	0.96	0.94	16	0.18	0.25	0.61	16	0.54	0.04	68	16	16
W11	1.13	2.70	0.26	70	0.35	0.96	0.56	16	0.18	0.32	0.49	14	0.41	0.02	70	16	14
W15pic	1.12	2.71	0.28	72	0.37	0.77	0.45	19	0.16	0.36	0.28	9	0.45	0.15	72	18	9
W15asb	1.13	2.71	0.27	78					0.2	0.42	0.51	22	0.26	0.09	78	0	23
W54asb	1.13	2.71	0.26	71					0.16	0.41	0.84	29	1.14	0.07	71	0	29
W54pic	1.13	2.69	0.27	59	0.35	0.75	1.13	30	0.18	0.41	0.29	11	0.45	0.15	59	30	11
W70pic	1.14	2.68	0.31	65	0.44	0.78	0.51	10	0.18	0.37	1.02	25	0.54	0.08	65	10	25
W96pic	1.13	2.69	0.29	65	0.28	0.88	0.86	27	0.19	0.29	0.24	8	0.88	0.09	65	27	8
J60-2	1.13	2.75	0.25	52	0.31	0.86	0.25	13	0.18	0.33	0.25	19	†	†	62	15	23
J68	1.14	2.72	0.27	31	0.34	0.77	0.81	69					2.72	0.98	31	69	0
Average	1.10	2.64			0.30	0.68			0.17	0.32			this study				
$\pm 2\sigma$	0.19	0.47			0.13	0.31			0.05	0.10							
Average	1.14	2.72			0.36	0.79			0.21	0.36			lizardite (O'Hanley & Dyar 1993)				
$\pm 2\sigma$	0.14	0.14			0.04	0.18			0.04	0.14							

* Abbreviations: %Mis: percent Misfit, %Uncrt: percent Uncertainty, as defined by Ruby (1973).

† Percent magnetite greater than 40% precludes the calculation of reliable fit parameters. Error bars on this fit are at least twice those given for pure samples.



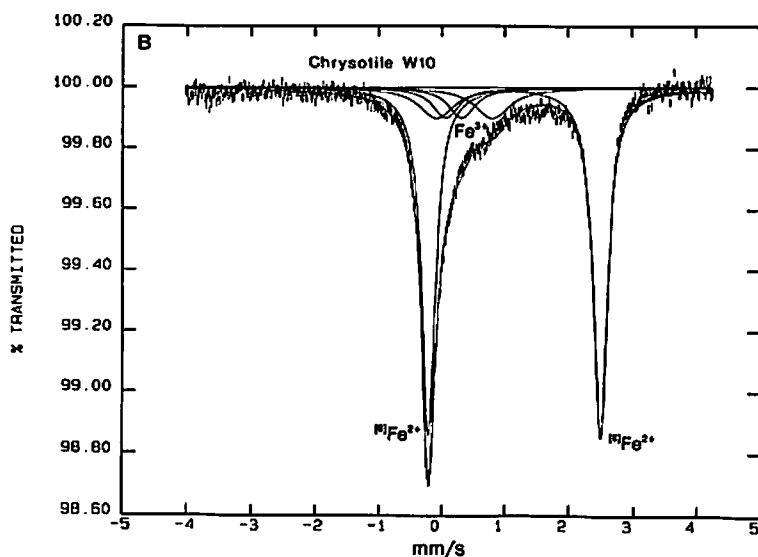


FIG. 2. Typical Mössbauer spectra of chrysotile. A. The spectrum for sample C54 exhibits shoulders at approximately 0.35 mm/s and 0.7 mm/s, indicative of the presence of significant amounts of both $^{54}\text{Fe}^{3+}$ and $^{56}\text{Fe}^{3+}$, respectively. B. The spectrum for sample W10 exhibits smaller shoulders, indicative of small amounts of both $^{54}\text{Fe}^{3+}$ and $^{56}\text{Fe}^{3+}$.

positive. On the basis of 18 atoms of oxygen, the proportion of H and excess charge show a strong negative correlation (Table 2).

CHRYSOTILE COMPOSITIONS AND SITE OCCUPANCIES

The compositions of the specimens of chrysotile used in this study are typical of this mineral (Wicks & Plant 1979). It has already been established that the range of composition in naturally occurring chrysotile is small, and that on average, chrysotile contains less Fe^{3+} and more Fe^{2+} than lizardite, but with considerable overlap at low levels of substitution (Whittaker & Wicks 1970, Wicks & Plant 1979). It is also known that chrysotile contains Fe^{3+} in tetrahedral coordination (Blauuw *et al.* 1979). However, variation in the site occupancy of Fe^{2+} and Fe^{3+} in chrysotile has not been studied in detail. Discussion here of the compositions of these chrysotile specimens will focus on variations in Si, Al, Cr, Mg, Fe^{3+} , and Fe^{2+} contents, because all other cations are present in amounts less than 0.01 atoms per 14 atoms of oxygen (Table 2).

The graph of $\{^{6}\text{Al} + ^{6}\text{Fe}^{3+} + \text{Cr}\}/\Sigma^{6}\text{I}$ versus $\{^{4}\text{Al} + ^{4}\text{Fe}^{3+}\}/\Sigma^{4}\text{I}$ (Fig. 3F) shows a positive correlation consistent with increasing amounts of trivalent cation substitution in both sheets of the structure. However, the regression line does not pass through the origin

and has a slope of 0.60, which suggests that there is a finite extent of incorporation of trivalent cations in the octahedra not accompanied by incorporation of trivalent cations in the tetrahedra. Starting with a Mg end-member composition, coupled substitution of trivalent cations for Si and Mg would generate a regression line passing through the origin with a slope of 0.68 (see Fig. 3F). Three considerations suggest that chrysotile has excess octahedral charge that can only reasonably be balanced by O-for-OH substitution, *i.e.*, vacancies in the hydrogen position: (1) the location of the data points with respect to such a line, (2) the excess charges based on 14 atoms of oxygen (Table 2), which are all positive but two (and these two have excess charges close to zero), and (3) the parameters for the regression line. The magnitude of the excess charge suggests the presence of 0.1 to 0.2 vacancies in the H site per 14 atoms of oxygen (Table 2).

The H^+ values show an inverse correlation with excess charge (Fig. 4A), consistent with a loss of H^+ and a gain of trivalent cations *via* the "oxybiotite" substitution ($\text{Fe}^{3+}\square\text{Fe}^{2+}_{-1}\text{H}^{+}_{-1}$). The inverse correlation is consistent with values for excess charge and trivalent cation contents determined without using the values for H_2O (Fig. 4B). Thus, the H^+ values, although they are low relative to excess charge, are consistent with vacancies in the H position of chrysotile.

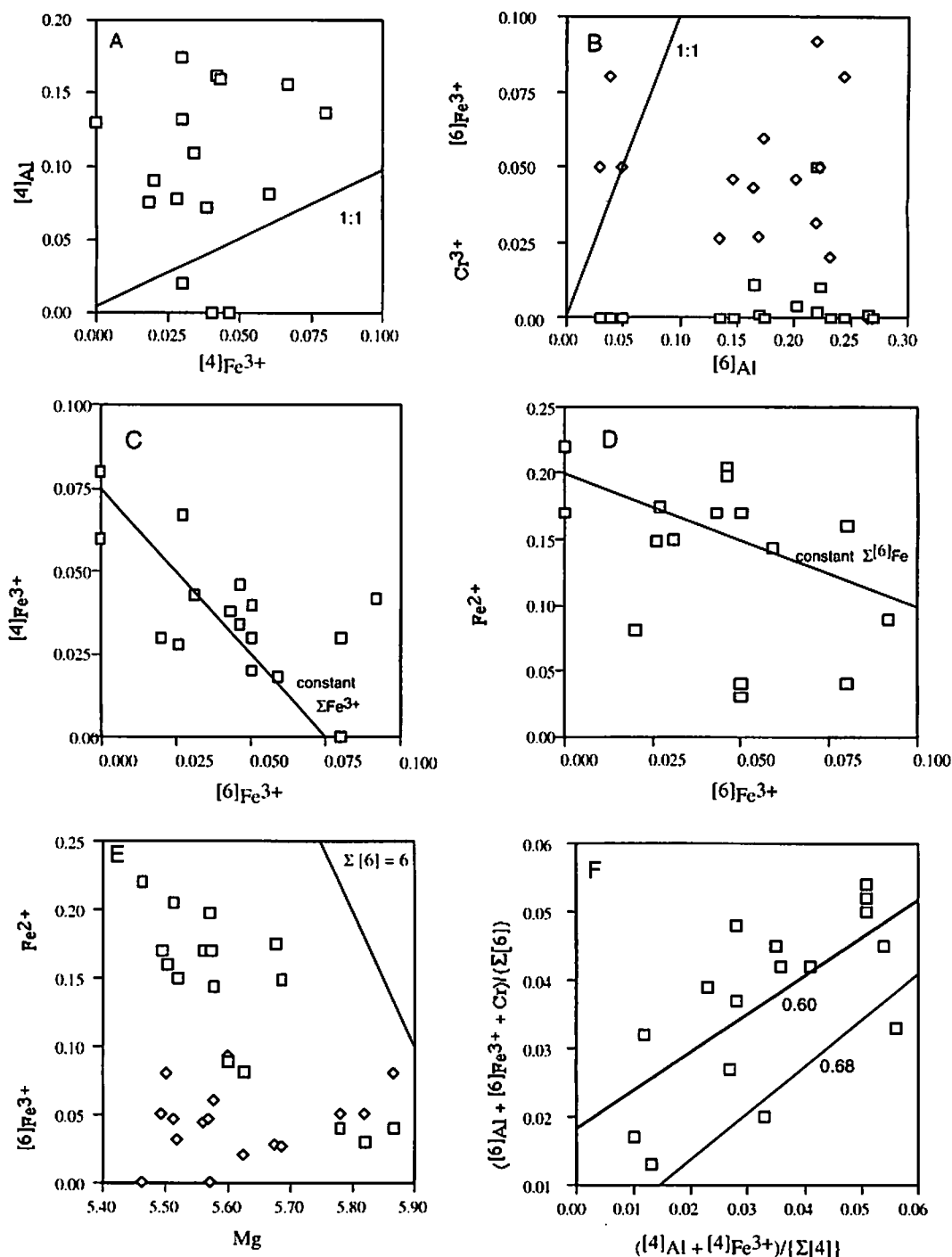


FIG. 3. Characteristics of the composition (atoms per 14 atoms of oxygen) of chrysotile specimens as determined in this study. A. $[4]\text{Al}$ versus $[4]\text{Fe}^{3+}$, with Al dominating over Fe^{3+} . B. Cr (□) or $^{16}\text{Fe}^{3+}$ (◇) versus $[6]\text{Al}$. C. $[4]\text{Fe}^{3+}$ versus $[6]\text{Fe}^{3+}$, with nearly constant total Fe^{3+} content. D. Fe^{2+} versus $[6]\text{Fe}^{3+}$. E. Fe^{2+} (□) or $^{16}\text{Fe}^{3+}$ (◇) versus Mg. F. $([6]\text{Al} + [6]\text{Fe}^{3+} + \text{Cr})/(\Sigma[6])$ versus $([4]\text{Al} + [4]\text{Fe}^{3+})/(\Sigma[4])$. Slope of the regression line is 0.60, and the intercept is non-zero. The value of 0.68 indicates change accompanying equal amounts of trivalent cation incorporation in both the octahedra and the tetrahedra.

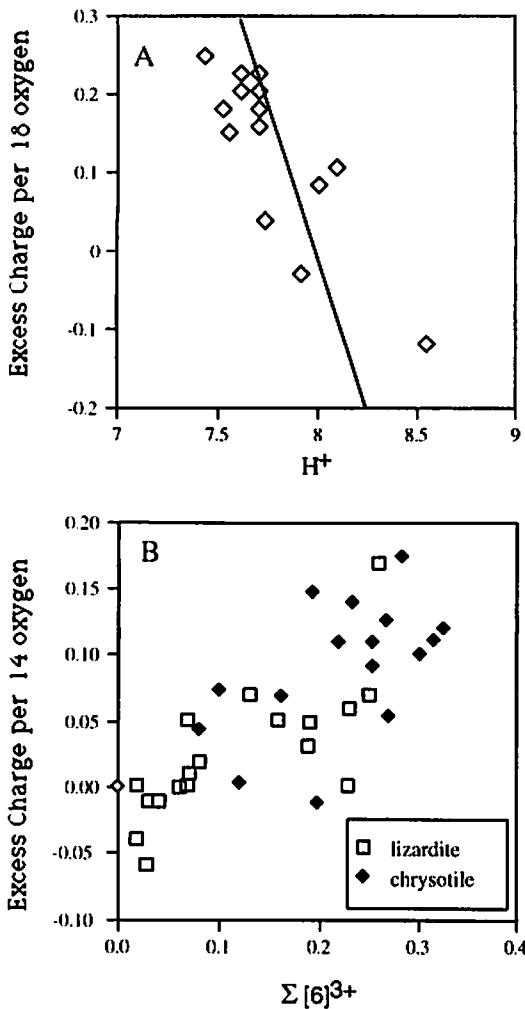


FIG. 4. A. Excess Charge versus H^+ (atoms per 18 atoms of oxygen). Line represents change away from an excess charge of zero at 8 H^+ . B. Excess charge (per 14 atoms of oxygen) versus octahedrally coordinated trivalent cations in lizardite and chrysotile.

COMPOSITIONS OF AND SITE OCCUPANCIES IN LIZARDITE

The compositional trends for lizardite-17 reported by O'Hanley & Dyar (1993) include: 1) both Al and Fe^{3+} as tetrahedrally coordinated cations, 2) an inverse correlation between $^{16}Fe^{3+}$ and Fe^{2+} , 3) a direct correlation between $^{14}Fe^{3+}$ and $^{16}Fe^{3+}$, 4) constant Fe^{2+}/Mg , and 5) no need to involve vacancies in the H position. These differences suggest the appropriate graphs to illustrate the differences in composition between lizardite and chrysotile.

Chrysotile contains both less Mg and shows more variation in amounts of Mg than does lizardite (Fig. 5A). Chrysotile tends to contain more Fe^{2+} for a given total Fe content than lizardite (Fig. 5B). The proportions of $^{14}Fe^{3+}$ and $^{16}Fe^{3+}$ show a negative correlation in chrysotile and a positive correlation in lizardite (Fig. 5C). Total Fe^{3+} content in chrysotile is nearly constant. The proportion of ^{14}Al is greater than $^{14}Fe^{3+}$ in chrysotile (Fig. 5D), whereas lizardite shows the opposite. Contents of $^{16}Fe^{3+}$ and Fe^{2+} (Fig. 6A), and values of Si/Mg (Fig. 6B) are similar in both minerals, although chrysotile displays slightly greater Si/Mg for a given Mg content. Chrysotile tends to contain smaller amounts of Fe^{3+} for a given Si content than does lizardite (Fig. 6C).

These changes can be summarized as follows. As $^{16}Fe^{3+}$ increases, chrysotile loses $^{14}Fe^{3+}$, whereas lizardite gains it. As Fe^{2+} content increases, lizardite loses Fe^{3+} from both tetrahedra and octahedra, whereas chrysotile loses $^{16}Fe^{3+}$ relative to $^{14}Fe^{3+}$. As Si content increases, lizardite loses Fe^{3+} from both tetrahedra and octahedra, whereas chrysotile either does not lose Fe^{3+} or shows a very slight increase.

The compositions of chrysotile and lizardite are also distinct within individual serpentinites. In the Woodsreef serpentinite, chrysotile contains more Fe^{2+} (Figs. 5A, B), Fe^{3+} (Fig. 5C), and ^{14}Al (Fig. 5D), and less Si (Fig. 6B) than lizardite. In the Cassiar serpentinite, chrysotile contains slightly more Fe^{2+} (Fig. 5B), more Si (Fig. 6C), and less $^{16}Fe^{3+}$ (Fig. 5C) and ^{14}Al (Fig. 5D) than lizardite. In the Jeffrey serpentinite, chrysotile contains more ^{14}Al (Fig. 5D), and less total Fe (Fig. 5B), Fe^{2+} (Fig. 5B), Fe^{3+} (Fig. 5C), and Si (Fig. 6C) than lizardite.

The extent of trivalent cation incorporation shows small differences in lizardite and chrysotile. In general, chrysotile shows a consistent excess of trivalent cation in the sheet of octahedra compared to lizardite (Fig. 6D).

The excess charge (per 14 atoms of oxygen) in lizardite takes on both positive and negative values that range between -0.06 and 0.17 (O'Hanley & Dyar 1993). In comparison, the excess charges on chrysotile vary from -0.03 to 0.19, with all but two being positive (Fig. 4B). Excess charge shows a positive correlation with increasing trivalent cation incorporation in the sheet of octahedra (Fig. 4B), with many samples of chrysotile plotting at higher values of excess charge. The data are consistent both with the idea that chrysotile requires vacancies in the H position to maintain charge neutrality, and with the inverse correlation between excess charge (based on 18 oxygen atoms) and H^+ content (Fig. 4A).

PHASE RELATIONS OF CHRYSOTILE AND LIZARDITE

The data on compositions of lizardite and chrysotile indicate that they are not polymorphs in natural

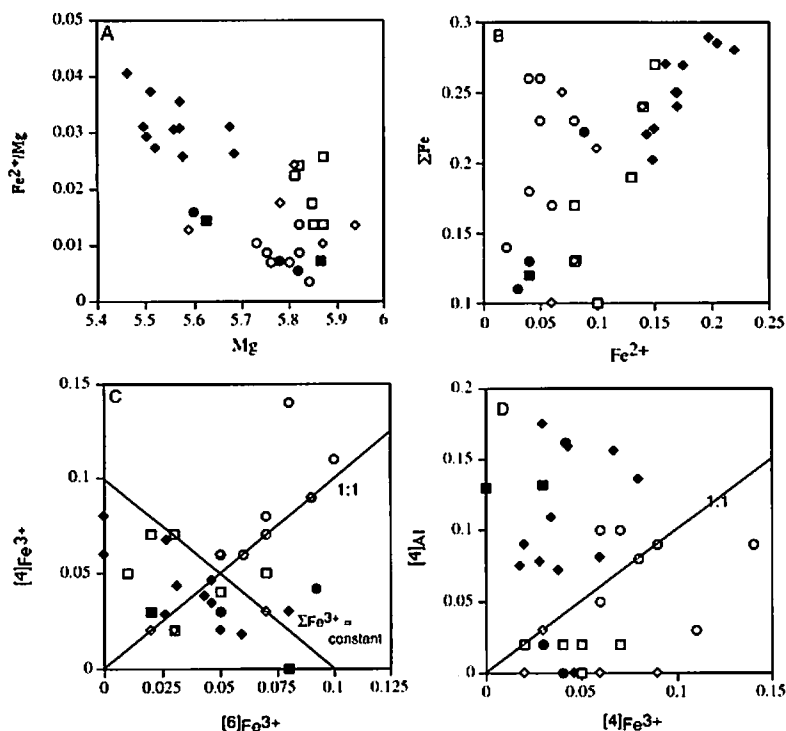


FIG. 5. Comparison of the compositions (in atoms per 14 atoms of oxygen) of lizardite and chrysotile (samples identified by mineral and deposit: lizardite samples from: (1) Woodsreef (\diamond), Cassiar (\circ), and Jeffrey (\square); chrysotile samples from: (1) Woodsreef (\blacklozenge), Cassiar (\bullet), and Jeffrey (\blacksquare)). A. Fe^{2+}/Mg versus Mg . Lizardite and chrysotile occupy distinct regions in the Fe^{2+}/Mg - Mg plane. B. Total Fe versus Fe^{2+} . C. $[4]\text{Fe}^{3+}$ versus $[6]\text{Fe}^{3+}$. The proportions of $[4]\text{Fe}^{3+}$ and $[6]\text{Fe}^{3+}$ are inversely correlated in chrysotile, preserving total Fe^{3+} content. The proportions of $[4]\text{Fe}^{3+}$ and $[6]\text{Fe}^{3+}$ are positively correlated in lizardite. D. $[4]\text{Al}$ versus $[4]\text{Fe}^{3+}$. Lizardite contains more $[4]\text{Fe}^{3+}$ than $[4]\text{Al}$, whereas chrysotile contains more $[4]\text{Al}$ than $[4]\text{Fe}^{3+}$.

systems. There are marked differences both if the data are considered as a whole, and also if they are considered within individual bodies of serpentinites. The compositional data presented above indicate that several exchange vectors operate in lizardite and chrysotile (Table 4). The vectors listed are selective, and supported by correlations among the data. For example, $[4]\text{Al}$ must be involved in an exchange vector that includes either Si or $[4]\text{Fe}^{3+}$ (or both), but the data do not indicate what the relation is, so it is not recorded in Table 4. The exchange vector FeMg_{-1} operates in both lizardite and chrysotile, but the other vectors are present either in one or the other. Note the inferred involvement of H^+ in the "oxybiotite" exchange vector $\text{Fe}^{2+}\text{H}^+\{[6]\text{Fe}^{3+}\}_{-1}$ in chrysotile. This vector is not needed for lizardite.

The relationships between the composition of lizardite and chrysotile are represented by a set

of equilibria, each of which focuses on a different cation (Table 4). The dominant points in these equilibria are: (1) the higher Fe^{2+} content of chrysotile compared to lizardite, (2) the inferred loss of H^+ from chrysotile, and (3) the higher $[4]\text{Al}$ content of chrysotile. The first equilibrium involves exchange of Fe^{2+} for Mg . The equilibrium is one of degree, in which chrysotile tends to contain more Fe^{2+} than lizardite, rather than lizardite being devoid of Fe^{2+} . The second equilibrium, the "oxybiotite" exchange vector, involves changes in the sheet of octahedra: a loss of H^+ is needed to compensate for the increased charge contributed by Fe^{3+} . It is written to conserve total Fe content. The third equilibrium describes the addition of Si for Fe^{3+} in the sheet of tetrahedra, and it involves a reduction in Fe^{3+} in the octahedra to maintain charge balance. The final equilibrium describes a complex exchange involving Al for Si , such that chrysotile contains more Al than Fe^{3+} .

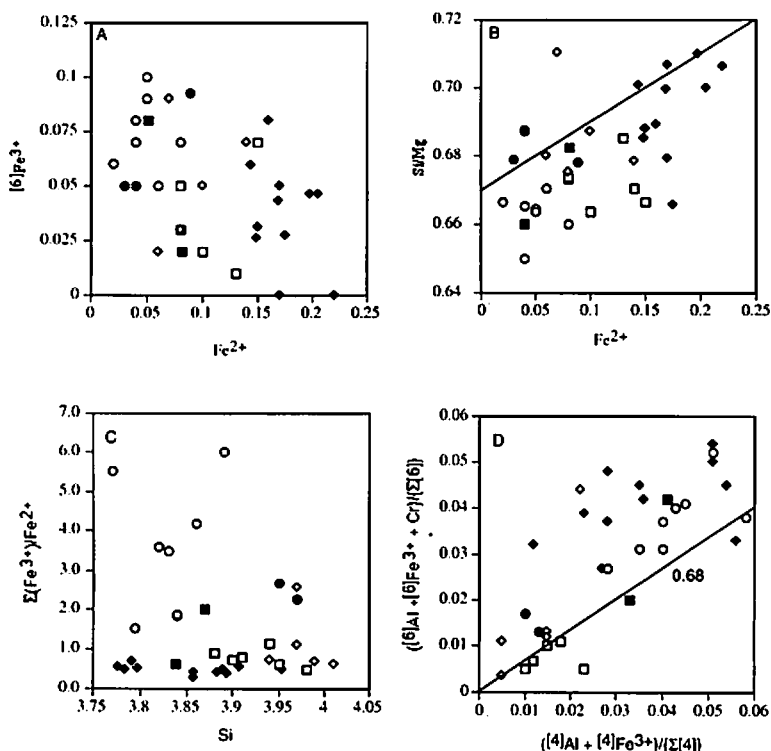


FIG. 6. Comparison of the compositions of lizardite and chrysotile. A. $[6]Fe^{3+}$ versus Fe^{2+} . B. Si/Mg versus Fe^{2+} . Line represents change in composition from Mg end-member ratio of 0.67 at 0 Fe^{2+} . C. $\Sigma Fe^{3+}/Fe^{2+}$ versus Si . D. $([6]Al + [6]Fe^{3+} + Cr)/\Sigma[6]$ versus $([4]Al + [4]Fe^{3+})/\Sigma[4]$. Line represents compositions resulting from substitution of equal amount of trivalent cations in both octahedra and tetrahedra.

in the tetrahedra, and the reduction in the proportion of octahedrally coordinated Fe^{3+} , such that chrysotile contains more Fe^{2+} than lizardite. The purpose of this equilibrium is to illustrate the effect of increased incorporation of Al on the oxidation state of Fe, rather than to imply that chrysotile contains more Al than lizardite. The existence of high-Al lizardite, which has no counterpart in chrysotile (Wicks & Plant 1979), suggests that the lizardite structure can accommodate more Al than can the chrysotile structure. We suggest, however, that the Tschermaks substitution $2AlMg_{-1}Si_{-1}$ describes the relations between low- and high-Al lizardite, not the exchange vector listed in Table 4.

The appropriate equilibria vary from one serpentinite to another. For example, in the Jeffrey serpentinite, chrysotile contains greater amounts of trivalent cations than lizardite (Fig. 6D), and this relation is described by the second and third equilibria in Table 4. At Woodsreef, chrysotile contains both more

Fe^{2+} (Figs. 5A, B, 6A) and $[4]Al$ (Fig. 5D) than lizardite. The first equilibrium describes the change of Fe^{2+} content, whereas the fourth equilibrium describes the change in Al content. The third equilibrium was used by O'Hanley & Dyar (1993) to describe the relation between lizardite composition and modal magnetite at Woodsreef. It can now be inferred that the same process that modified the composition of lizardite led eventually to the replacement of lizardite by chrysotile. In contrast, in the Cassiar serpentinite, chrysotile has both lower total Fe^{3+} (Fig. 5B) and lower $[6]Fe^{3+}$ (Fig. 5C) than lizardite. These differences are described by the second and third equilibria in Table 4.

In the four serpentinites exhibiting evidence for serpentine replacement studied thus far (Vimy Ridge; Cogulu & Laurent 1984; Woodsreef; O'Hanley & Offler 1992; Jeffrey; O'Hanley & Wicks 1990; Cassiar; O'Hanley & Wicks 1995), the reactions involving the replacement of lizardite by chrysotile and *vice versa* are

TABLE 4. EXCHANGE VECTORS IN LIZARDITE AND CHRYSOTILE, AND EQUILIBRIA DESCRIBING THE RELATIONS BETWEEN THEM

Lizardite*	Chrysotile	Reference
FeMg_3	FeMg_3	Fig. 3E
$\text{Fe}^{2+}\text{Si}^{4+}[\text{Fe}^{3+}]_n[\text{Fe}^{2+}]_{3-n}$	$[\text{Fe}^{3+}]_n[\text{Fe}^{2+}]_{3-n}$	Fig. 3C
	$\text{Fe}^{2+}\text{H}^{+}[\text{Fe}^{3+}]_{n-1}$	Fig. 3D, 4
Equilibria between lizardite and chrysotile†		
Exchange of Mg for Fe $\text{Mg}_3\text{Si}_2\text{O}_5(\text{OH})_4 + 3 \text{Fe}(\text{OH})_2 = \text{Fe}^{2+}_3\text{Si}_2\text{O}_5(\text{OH})_4 + 3 \text{Mg}(\text{OH})_2$		
		Fig. 5A
Change of both oxidation state of Fe and H^+ content of octahedral sheet $\text{Fe}^{2+}_3\text{Si}_2\text{O}_5(\text{OH})_4 = \text{Fe}^{3+}_3\text{Fe}^{2+}\text{Si}_2\text{O}_5(\text{OH})_4 + \frac{1}{2} \text{H}_2$		
		See text
Change in both total Fe content and oxidation state of Fe $\text{Fe}^{2+}_3\text{Fe}^{3+}\text{Si}_2\text{O}_5(\text{OH})_4 + \text{Si}(\text{OH})_4 + \frac{3}{2} \text{H}_2 =$ $\text{Fe}^{2+}_3\text{Si}_2\text{O}_5(\text{OH})_4 + \frac{1}{2} \text{Fe}_2\text{O}_3 + \frac{1}{2} \text{H}_2\text{O}$		
		Figs. 5B, 5C
Change in both trivalent cations and H^+ contents at constant total Fe $\text{Fe}^{2+}_3\text{Fe}^{3+}_n\text{Al}_n\text{Si}_2\text{O}_5(\text{OH})_4 + \frac{1}{2} \text{Al}(\text{OH})_3 + \frac{1}{2} \text{H}_2\text{O} =$ $\text{Fe}^{2+}_3\text{Fe}^{3+}_n\text{AlSi}_6\text{O}_8(\text{OH})_4 + \frac{1}{2} \text{Si}(\text{OH})_4 + \frac{1}{4} \text{H}_2$		
		Figs. 5B, 5C

* from O'Hanley & Dyar (1993).

† Equilibria are written with lizardite on the left-hand side and chrysotile on the right-hand side of the equal sign.

all different. These differences are attributed to the actions of distinct fluids present during serpentinization. Such differences suggest that there are several changes in composition that result in the replacement of lizardite by chrysotile (with or without involvement of other minerals). The equilibria given in Table 4 can account for the effects of fluid composition in that lizardite can be replaced by chrysotile if: 1) more Fe^{2+} is available (first equilibrium), 2) more Si for "Fe-rich" compositions (third equilibrium), 3) more Al for "Fe-" and "Al-rich" compositions (fourth equilibrium), and 4) either less (third equilibrium) or more (second and fourth equilibria) oxidizing conditions. Furthermore, it is probable that none of these equilibria work (with the exception of the second one) in isolation because of the overlap in compositions of lizardite and chrysotile. Furthermore, all of these changes can occur at constant temperature.

CONCLUSIONS

Lizardite and chrysotile are not polymorphs in natural systems, and attempts to understand their behavior in natural systems based on Mg end-member compositions will not be successful. It is probable that the transition from lizardite to chrysotile in natural

systems is caused by a loss of H^+ accompanying the substitution of Fe^{3+} for Fe^{2+} or Mg, such that the presence of Fe^{2+} results in curving of the structure in chrysotile. The complexity and number of the proposed equilibria relating lizardite to chrysotile imply that there are many potential paths to form chrysotile from lizardite (and *vice versa*). Thus, the replacement of lizardite by chrysotile in a given serpentinite cannot be explained *a priori*, making a detailed study of its paragenesis necessary.

ACKNOWLEDGEMENTS

We thank Kurt Kyser (Queen's University) and Tom Bonli (University of Saskatchewan) for access to and assistance with the electron microprobe, and Michael Colucci, Kurt Ferguson, and Robert Gregory (Southern Methodist University) for access to and assistance with hydrogen determinations. We also thank Andrew Zingg (Büro für Hydrogeologie und Geotechnik) and Mark van Baalen (Harvard University) for reading the manuscript. We thank Editor Robert Martin, Associate Editor Frank Hawthorne, an anonymous reviewer, and Joe Chernosky for editorial assistance.

REFERENCES

- BIGEISEN, J., PERLMAN, M.L. & PROSSER, H.C. (1952): Conversion of hydrogenic materials to hydrogen for isotopic analysis. *Anal. Chem.* **24**, 1356-1357.
- BLAUW, C., STROINK, G., LEIPER, W. & ZENTILLI, M. (1979): Mössbauer analysis of some Canadian chrysotiles. *Can. Mineral.* **17**, 713-717.
- COGULU, E. & LAURENT, R. (1984): Mineralogical and chemical variations in chrysotile veins and peridotite host-rocks from the asbestos belt of southern Québec. *Can. Mineral.* **22**, 173-183.
- EVANS, B.W., JOHANNES, W., OTTERDOOM, H. & TROMMSDORFF, V. (1976): Stability of chrysotile and antigorite in the serpentinite multisystem. *Schweiz. Mineral. Petrogr. Mitt.* **56**, 79-93.
- GLEN, R.A. & BUTT, B.C. (1981): Chrysotile asbestos at Woodsreef, New South Wales. *Econ. Geol.* **76**, 1153-1169.
- GRANT, C.A. (1995): *Sources of Experimental and Analytical Error in Measurements of the Mössbauer Effect in Amphibole*. Ph.D. thesis, Univ. of Oregon, Eugene, Oregon.
- HOLDAWAY, M.J., DUTROW, B.L., BORTHWICK, J., SHORE, P., HARMON, R.S. & HINTON, R.W. (1986): H content of staurolite as determined by H extraction line and ion microprobe. *Am. Mineral.* **71**, 1135-1141.
- LONG, G.J., CRANSHAW, T.E. & LONGWORTH, G. (1984): The ideal Mössbauer absorber thickness. *Mössbauer Effect Data J.* **6**, 42-49.
- MELLINI, M., TROMMSDORFF, V. & COMPAGNONI, R. (1987): Antigorite polysomatism: behavior during progressive metamorphism. *Contrib. Mineral. Petrol.* **97**, 147-155.
- _____ & ZUSSMAN, J. (1986): Carlosturanite (not 'picrolite') from Taberg, Sweden. *Mineral. Mag.* **50**, 675-679.
- O'HANLEY, D.S. (1991): Fault-controlled phenomena associated with hydration and serpentine recrystallization during serpentinization. *Can. Mineral.* **29**, 21-35.
- _____ & DYAR, M.D. (1993): The composition of lizardite 1T and the formation of magnetite in serpentinites. *Am. Mineral.* **78**, 391-404.
- _____ & OFFLER, R. (1992): Characterization of multiple serpentinization, Woodsreef, New South Wales. *Can. Mineral.* **30**, 1113-1126.
- _____ & WICKS, F.J. (1990): A method for the determination of fiber quality. The Asbestos Institute, Montréal, Québec.
- _____ & _____ (1995): Conditions of formation of lizardite, chrysotile and antigorite, Cassiar, British Columbia. *Can. Mineral.* **33**, 753-773.
- _____, SCHANDL, E.S. & WICKS, F.J. (1992): The origin of rodingites from Cassiar, British Columbia, and their use to estimate T and P(H₂O) during serpentinization. *Geochim. Cosmochim. Acta* **56**, 97-108.
- SKOGBY, H., ANNERSTEN, H., DOMENEGHETTI, M.C., MOLIN, G.M. & TAZZOLI, V. (1992): Iron distribution in orthopyroxene: a comparison of Mössbauer spectroscopy and X-ray refinement results. *Eur. J. Mineral.* **4**, 441-452.
- WHITTAKER, E.J.W. & WICKS, F.J. (1970): Chemical differences among the serpentine "polymorphs": a discussion. *Am. Mineral.* **55**, 1025-1047.
- _____ & ZUSSMAN, J. (1956): The characterization of serpentine minerals by X-ray diffraction. *Mineral. Mag.* **31**, 107-126.
- WICKS, F.J. (1979): Mineralogy, crystal chemistry and crystallography of chrysotile. In *Mineralogical Techniques of Asbestos Determination* (R.L. Ledoux, ed.). *Mineral. Assoc. Can., Short-Course Handbook* **4**, 35-78.
- _____ & PLANT, A.G. (1979): Electron microprobe and X-ray-microbeam studies of serpentine textures. *Can. Mineral.* **17**, 785-830.
- _____ & ZUSSMAN, J. (1975): Microbeam X-ray diffraction patterns of the serpentine minerals. *Can. Mineral.* **13**, 244-258.

Received April 4, 1997, revised manuscript accepted March 31, 1998.